ELSEVIER

Physica C 332 (2000) 40–44

PHYSICA C

www.elsevier.nl/locate/physc

Dynamic phase diagram and orientational dependence for vortices in superconductors with periodic arrays of pinning sites

Franco Nori [a,*], C. Reichhardt [b]

[a] *Department of Physics, The University of Michigan, Ann Arbor, MI 48109-1120, USA*
[b] *Department of Physics, University of California, Davis, CA 95616, USA*

Abstract

We investigate the depinning and dynamics of vortex lattices at incommensurate fields above the first matching field. The vortex lattice interacts with periodic pinning arrays for different angles of vortex driving with respect to the pinning lattice. We find that the optimal pinning for square arrays of pins occurs for drives at 45° with respect to the pinning lattice. We present a dynamic phase diagram and show the evolution of these dynamic phases as a function of driving angle with respect to the pinning lattice.

Keywords: Dynamic phase diagram; Pinning sites; Vortex lattices

1. Introduction

Driven vortices interacting with quenched disorder represent an ideal system in which to study driven nonequilibrium systems with many degrees of freedom. Theoretical [1–14] and experimental work [15–19] have produced considerable evidence that these systems can exhibit *dynamic phase transitions* between different vortex flow states. For systems with random quenched disorder there is evidence for a pinned phase, plastic flow, moving smectic, and moving crystal phases. The distinct phases are characterized by the vortex lattice structure and the vortex trajectories. In the plastic flow phase, the highly disordered vortex lattice flows in winding channels. In the moving smectic phase, the lattice flows in uncorrelated 1D channels, while in the moving crystal phase, it follows correlated 1D channels and is nearly defect free. Recently, simulations for systems with periodic pinning have found a particularly rich variety of dynamical phases [20–22].

An interesting aspect of periodic pinning that is absent in random disorder is that the pinning properties and the dynamic phases themselves should depend on the angle of drive with respect to the symmetry direction of the pinning lattice. The initial depinning and subsequent flow phases for low driving forces for a vortex lattice driven at varied angles with respect to the symmetry angle of the periodic pinning lattice has so far not been studied. Recently, the locked phases for the highly driven case, where the entire vortex lattice is moving, have been studied with numerical simulations [22]. There it was found that the vortex lattice locks into certain directions that are commensurate with the symmetry of the underlying pinning lattice. The low-driving case is relevant not only for the effect on the vortex dynam-

* Corresponding author. Fax: +1-734-7639694.
E-mail address: nori@umich.edu (F. Nori).

0921-4534/00/$ - see front matter
PII: S0921-4534(99)00641-3

ics, but also has relevance for the optimal pinning of vortices since it is likely that the critical current will vary with the angle of drive.

Periodic pinning arrays have been attracting increasing interest as various lithographic techniques have been applied to create well-defined arrays of microholes or ''antidots'' [23–31] and magnetic dot arrays [32–36]. In these systems, interesting commensurability effects have been observed with bulk experimental measures [23–30,32–36], direct imaging [31] and simulations [37]. The vortex configurations and pinning force at the commensurate or matching fields depend on the symmetry of the pinning lattice as well as the size of the individual pinning sites. For small pinning sites, where only one vortex is trapped per pinning site, transport measurements [30] and the appearance of Shapiro steps at the second matching field offer strong evidence that the initial depinning transition occurs by the flow of interstitial vortices while the rest of the vortices remain immobile at the pinning sites.

In this work, we study the dependence of the critical current and vortex dynamics on the angle of the drive of the vortex lattice with respect to the symmetry axis of the pinning lattice. When interstitial vortices are present, we observe that the optimal pinning occurs when the vortex lattice is driven at 45° with respect to the pinning lattice. For certain angles we find that the flow does not consist of interstitial vortices flowing between pinned vortices, but instead occurs along the pinning rows or as a random plastic flow phase. We show how these dynamic plastic flow phases can be experimentally distinguished with current–voltage curves. We also present a dynamic phase diagram for angle-of-drive vs. driving force.

2. Approach used

We numerically integrate the overdamped equation of motion:

$$f_i = f_i^{vv} + f_i^{vp} + f_d = \eta \boldsymbol{v}_i. \quad (1)$$

Here the total force acting on vortex i is f_i and we take $\eta = 1$. The force from the other vortices is $f_i^{vv} = \sum_{j=1}^{N_v} f_0 K_1(|\boldsymbol{r}_i - \boldsymbol{r}_j|/\lambda)\hat{\boldsymbol{r}}_{ij}$. Here $K_1(r/\lambda)$ is a modified Bessel function and λ is the penetration depth, $f_0 = \Phi_0^2/8\pi^2\lambda^3$, and $\hat{\boldsymbol{r}}_{ij} = (\boldsymbol{r}_i - \boldsymbol{r}_j)/|\boldsymbol{r}_i - \boldsymbol{r}_j|$. Since the Bessel function falls off exponentially for $r > \lambda$, a cutoff can be safely placed at $r = 6\lambda$ for computational efficiency. The pinning is modeled as attractive parabolic wells with $f_i^{vp} = (f_p/r_p)\Theta(|\boldsymbol{r}_i - \boldsymbol{r}_k^{(p)}|/\lambda)\hat{\boldsymbol{r}}_{ik}^{(p)}$. Here Θ is the Heaviside step function, $\boldsymbol{r}_k^{(p)}$ is the location of pinning site k, f_p is the maximum pinning force, and $\hat{\boldsymbol{r}}_{ik}^{(p)} = |\boldsymbol{r}_i - \boldsymbol{r}_k^{(p)}|/|\boldsymbol{r}_i - \boldsymbol{r}_k^{(p)}|$. The pinning is placed in a square array. We consider a density of vortices of $N_v = 1.07N_p$, so that each of the pinning sites are filled with one vortex and the rest of the vortices sit in the interstitial regions between the pinning sites. The driving force f_d, representing the Lorentz force from an applied current, is decomposed into its Cartesian coordinates, f_x and f_y, with the total magnitude of $f_d = (f_x^2 + f_y^2)^{1/2}$. We consider the symmetry direction of the square pinning lattice to be the x direction. As a function of f_d we measure the net velocity of the vortex lattice in the x-direction, $V_x = \sum_{i=1}^{N_v} \boldsymbol{v}_i \cdot \hat{\boldsymbol{x}}$, and y direction, $V_y = \sum_{i=1}^{N_v} \boldsymbol{v} \cdot \hat{\boldsymbol{y}}$. All lengths, fields and forces are given in units of λ, Φ_0/λ^2 and f_0. In this work $r_p = 0.3\lambda$, and the density of pinning sites is $n_p = 0.28\Phi_0/\lambda^2$.

3. *I–V* curves

In Fig. 1, we plot the Cartesian coordinates, V_x and V_y, of the average vortex velocity, for varying angles of drive. In Fig. 1(a), for $\theta = 0$, $V_y = 0$ and V_x shows a series of jumps which correspond to transitions in the vortex flow patterns. These different flow phases for the driving in the x-direction are described in detail in Refs. [20,21]. For low drives $f_x/f_0 < 0.175$, all the vortices are pinned, and we label this state phase I. The initial motion of vortices as indicated by the increases in V_x at $f_x/f_0 = 0.155$ occurs by the motion of interstitial vortices between the pinning sites which is referred to as phase II flow.

The jump in V_x at $f_x/f_0 = 0.325$ corresponds to the transition to phase IV flow, where a portion of the vortices move *along* the rows of pinning and the vortex motion occurs in a pulsed or soliton-like manner; with ''discommensurations'' moving much faster than the average vortex velocity. Finally, in phase V, for $f_x/f_0 > 0.5$, the entire vortex lattice

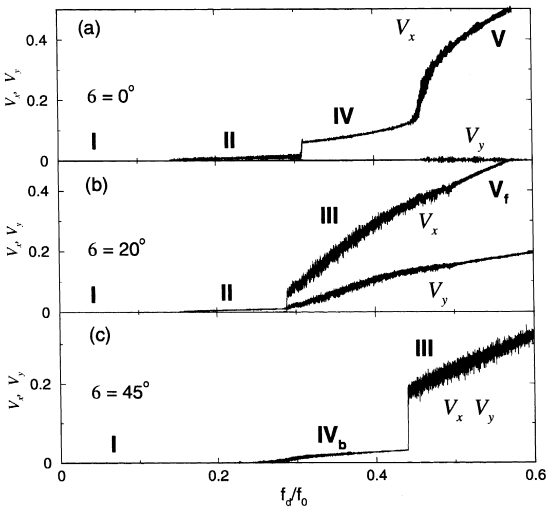

Fig. 1. Cartesian components, V_x and V_y, of the average vortex velocity for a system with periodic pinning where $B = 1.06B_\phi$, $B_\phi = 0.28\Phi_0/\lambda^2$, $f_p/f_0 = 0.5$, $r_p = 0.3\lambda$, driven at different angles θ. (a) $\theta = 0°$, (b) $\theta = 20°$, (c) $\theta = 45°$. In (c), $V_x = V_y$.

starts flowing with the motion still strictly along the pinning rows. In Fig. 1(b) for $\theta = 20°$, phase I has grown and phase IV is lost. The initial vortex motion is still strictly in the x-direction in phase II; however, near $f_d = 0.3$, there is a jump in V_x and V_y becomes nonzero. This jump corresponds to the onset of a plastic flow phase, labeled phase III, where the vortex lattice flows in irregular patterns and exhibits disorder. The V_y and V_x in phase III show increased fluctuations. For $f_d > 0.5$, the fluctuations in V_x and V_y decrease and the vortex lattice reorders. We label this phase V_f flow. The vortex lattice structure in this phase depends strongly on θ and is discussed more thoroughly in Ref. [22]. In Fig. 1(c), for $\theta = 45°$, $V_x = V_y$ for all f_d. Here the pinned phase phase I is seen to be considerably larger than at $\theta = 0$, with $f_c(45°)/f_c(0°) = 1.8$. At $f_d/f_0 = 0.25$, the lattice depins and begins moving at 45°, as indicated by the equal increase in V_x and V_y. The vortex motion in this phase is very similar to phase IV, where vortex motion occurs by soliton-like motion of discommensurations along the pinning rows, except here the vortices move along at a 45° angle. The vortex lattice then enters phase III as indicated by the large jump in V_x and V_y. For $f_d/f_0 > 0.5$, the vortex lattice reorders to what we label phase V_b flow, with the vortices now flowing strictly along the pinning sites at 45°.

In Fig. 2, we plot the vortex trajectories for the various phases. In Fig. 2(a), the phase II vortex motion follows 1D channels where the interstitial vortices move along the x direction between the pinned vortices. In Fig. 2(b), the phase IV flow is restricted to 1D channels along the pinning rows. Only rows containing extra vortices are mobile. In Fig. 2(c), phase III for $\theta = 20°$, the vortices move in a random-like manner. Note that the vortices show a tendency to move at 20°. In Fig. 2(d), in phase IV_b, we find a similar flow of vortices along 1D channels that contain extra vortices while the commensurate rows remain pinned as in the phase IV flow, but here the vortices move along at 45°.

The vortex lattice also exhibits a variety of different structures associated with the different dynamic

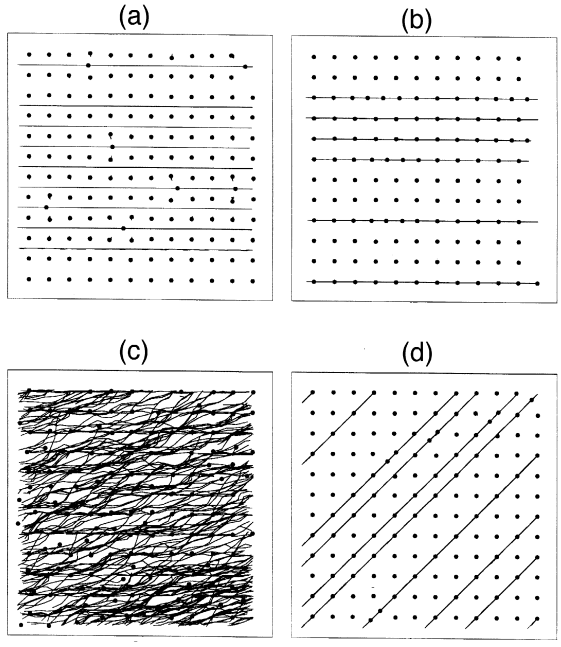

Fig. 2. The vortex flow trajectories for (a) phase II, with interstitial flow of vortices between the vortices at the pinning sites. (b) Phase IV flow where the vortices flow along the pinning rows. Only rows with an incommensurate number of vortices are mobile. (c) Phase III flow for $\theta = 20°$ showing a winding disordered motion of vortices. (d) Phase IV_b flow where the vortices move along the pinning rows in a manner similar to phase IV flow except that here the motion is along 45°.

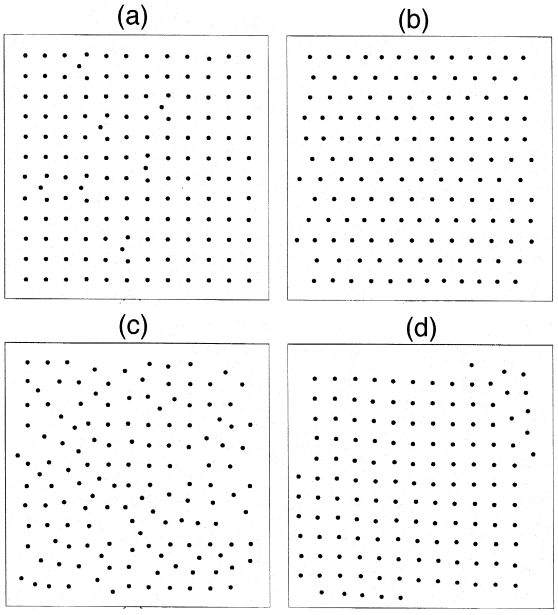

Fig. 3. The vortex positions for (a) phase II flow showing that the overall vortex lattice is square with some vortices located in the interstitial regions. (b) Vortex positions for phase V. Here the overall vortex lattice has some triangular order. Certain rows have a higher number of vortices than the other rows. (c) Phase III flow showing a disordered vortex lattice. (d) Phase V_b flow showing a square vortex lattice.

phases. In Fig. 3, we show the instantaneous vortex structures for several phases. In Fig. 3(a), during the dynamic phase II flow, the vortex lattice is square with some interstitial vortices located between a portion of the pinned vortices. In Fig. 3(b), the highly driven phase V for driving along the *x*-axis, the vortex lattice is more *triangular* with an absence of any interstitial vortices as in phase II. Fig. 3(c) shows phase III, where the vortex lattice is highly disordered. In Fig. 3(d), the vortex structure for phase V_b shows that the vortex lattice is mostly *square* and rotated at 45° with respect to the pinning lattice. This is in contrast with the phase V flow where the vortex lattice has a more triangular ordering.

4. Dynamic phase diagram for different orientations

In Fig. 4, we present the main results of this work, in a phase diagram for f_d vs. θ obtained by conducting a series of simulations for different θ. The different phases are identified from the *V–I* characteristic and vortex lattice structures. The pinned phase phase I is smallest for driving along the *x*-direction and increases to a maximum at $\theta = 45°$. The phase II flow is largest for $\theta = 0$ and gradually decreases, disappearing for $\theta > 40°$. The increase in the driving force at which depinning occurs as θ increases can be understood by considering that the depinning transition is determined by the onset of motion for the interstitial vortices. These vortices are pinned not directly from the pinning sites themselves but by the interaction with the vortices at the pinning sites. For $\theta = 0$, the interstitial vortex motion occurs strictly between the pinning. The largest depinning current should occur near $\theta = 45$ since an interstitial vortex must depin a pinned vortex in order to move.

We have also found that for triangular pinning arrays, certain angles of driving such as $\theta = 0$ and $\theta = 60°$ produce the maximum pinning for interstitial vortices since at these angles the interstitial vortices move directly into the vortices at the pinning sites. The disappearance of phase II can be understood by considering that for large enough θ the interstitial vortices depin the vortices at the pinning sites which in turn depin the next pinned vortices, leading to phase IV_b motion. For $\theta < 10°$, all the vortex motion occurs strictly in the *x*-direction. For angles greater than 10° phases IV and V are lost and phase III

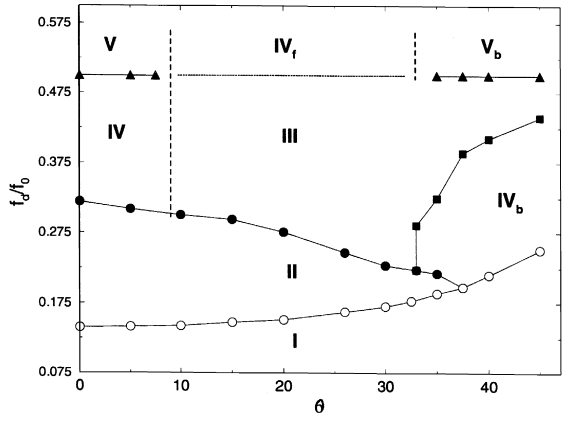

Fig. 4. The dynamic phase diagram for the driving force f_d vs. θ. As θ increases, phase I, or the critical depinning force, also increases to a maximum at 45°. Phases IV and V only occur for $\theta < 10°$. Phases IV_b and V_b appear for $\theta > 33°$.

appears. For $\theta > 33°$ phase IV_b appears. For increasing f_d there is a transition from phase IV_b to phase III. This transition increases to higher f_d for increasing θ reaching a maximum at $\theta = 45°$. Phase V_b occurs for $f_d/f_0 > 0.5$ and $\theta > 33°$.

5. Summary

In summary, we have investigated the vortex depinning and dynamics in superconductors with periodic pinning arrays for the case where interstitial vortices are present for varying angles of drive with respect to the pinning lattice. We observe the evolution of the dynamic phases for increasing drive. The onset of the different phases can be observed as clear jumps or features in the transverse and longitudinal V–I curves. We find that the maximum pinning occurs for drives along 45° with respect to the pinning lattice. We summarize our results in a dynamic phase diagram of the angle of drive θ vs. driving force f_d.

References

[1] F. Nori, Science 271 (1996) 1373.
[2] C. Reichhardt et al., Phys. Rev. B 53 (1996) R8898.
[3] A.E. Koshelev, V.M. Vinokur, Phys. Rev. Lett. 73 (1994) 3580.
[4] K. Moon, R.T. Scalettar, G.T. Zimanyi, Phys. Rev. Lett. 77 (1996) 2778.
[5] S. Ryu et al., Phys. Rev. Lett. 77 (1996) 5114.
[6] M.C. Faleski, C. Marchetti, A.A. Middleton, Phys. Rev. B 54 (12) (1996) 427.
[7] C.J. Olson, C. Reichhardt, F. Nori, Phys. Rev. B 56 (1997) 6175.
[8] C.J. Olson et al., Physica C 290 (1997) 89.
[9] S. Spencer, H.J. Jensen, Physica C 55 (1997) 8473.
[10] C.J. Olson, C. Reichhardt, F. Nori, Phys. Rev. Lett. 81 (1998) 3757.
[11] D. Dominguez, Phys. Rev. Lett. 82 (1999) 181.
[12] T. Giamarchi, P. Le Doussal, Phys. Rev. B 57 (1998) 11356.
[13] L. Balents, M.C. Marchetti, L. Radzihovsky, Phys. Rev. B 57 (1998) 7705.
[14] S. Scheidl, V.M. Vinokur, Phys. Rev. E 57 (1998) 2574.
[15] S. Bhattacharya, M.J. Higgins, Phys. Rev. Lett. 70 (1993) 2617.
[16] U. Yaron et al., Nature 376 (1995) 753.
[17] W. Henderson et al., Phys. Rev. Lett. 77 (1996) 2077.
[18] F. Pardo et al., Nature 396 (1998) 348.
[19] A.M. Troyanovski, J. Aarts, P.H. Kes, Nature 399 (1999) 665.
[20] C. Reichhardt, C.J. Olson, F. Nori, Phys. Rev. Lett. 78 (1997) 2648.
[21] C. Reichhardt, C.J. Olson, F. Nori, Phys. Rev. B 58 (1998) 6534.
[22] C. Reichhardt, F. Nori, Phys. Rev. Lett. 82 (1999) 414.
[23] M. Baert et al., Phys. Rev. Lett. 74 (1995) 3269.
[24] J.Y. Lin et al., Phys. Rev. B 54 (R12) (1996) 714.
[25] A. Bezryadin, Yu.B. Ovchinnikov, B. Pannetier, Phys. Rev. B 53 (1996) 8553.
[26] A. Castellanos et al., Appl. Phys. Lett. 71 (1997) 962.
[27] V.V. Metlushko et al., Europhys. Lett. 41 (1998) 333.
[28] V.V. Moshchalkov et al., Phys. Rev. B 57 (1998) 3615.
[29] V.V. Metlushko et al., Phys. Rev. B 59 (1999) 603.
[30] E. Rosseel et al., Phys. Rev. B 53 (1996) R2983.
[31] K. Harada et al., Science 271 (1996) 1393.
[32] J.I. Martín et al., Phys. Rev. Lett. 79 (1997) 1929.
[33] D.J. Morgan, J.B. Ketterson, Phys. Rev. Lett. 80 (1998) 3614.
[34] Y. Jaccard et al., Phys. Rev. B 58 (1998) 8232.
[35] M.J. Van Bael et al., Phys. Rev. B 59 (1999) 14674.
[36] J.I. Martín et al., Phys. Rev. Lett. 83 (1999) 1022.
[37] C. Reichhardt, C.J. Olson, F. Nori, Phys. Rev. B 57 (1998) 7937.